Molecular Biology of the Cell
Vol. 16, 141–152, January 2005

Analysis of a Spindle Pole Body Mutant Reveals a Defect in Biorientation and Illuminates Spindle Forces[D] [V]

Tennessee J. Yoder,*† Mark A. McElwain,* Susan E. Francis,* Joy Bagley,*† Eric G.D. Muller,* Brian Pak,‡ Eileen T. O'Toole,‡ Mark Winey,‡ and Trisha N. Davis*†§

*Department of Biochemistry and †Program in Molecular and Cellular Biology, University of Washington, Seattle, WA 98195; and ‡Department of Molecular, Cellular and Developmental Biology, University of Colorado, Boulder, CO 80309

Submitted August 16, 2004; Accepted October 25, 2004
Monitoring Editor: Tim Stearns

The spindle pole body (SPB) is the microtubule organizing center in *Saccharomyces cerevisiae*. An essential task of the SPB is to ensure assembly of the bipolar spindle, which requires a proper balancing of forces on the microtubules and chromosomes. The SPB component Spc110p connects the ends of the spindle microtubules to the core of the SPB. We previously reported the isolation of a mutant allele *spc110–226* that causes broken spindles and SPB disintegration 30 min after spindle formation. By live cell imaging of mutant cells with green fluorescent protein (GFP)-Tub1p or Spc97p-GFP, we show that *spc110–226* mutant cells have early defects in spindle assembly. Short spindles form but do not advance to the 1.5-μm stage and frequently collapse. Kinetochores are not arranged properly in the mutant cells. In 70% of the cells, no stable biorientation occurs and all kinetochores are associated with only one SPB. Examination of the SPB remnants by electron microscopy tomography and fluorescence microscopy revealed that the Spc110–226p/calmodulin complex is stripped off of the central plaque of the SPB and coalesces to from a nucleating structure in the nucleoplasm. The central plaque components Spc42p and Spc29p remain behind in the nuclear envelope. The delamination is likely due to a perturbed interaction between Spc42p and Spc110–226p as detected by fluorescence resonance energy transfer analysis. We suggest that the force exerted on the SPB by biorientation of the chromosomes pulls the Spc110–226p out of the SPB; removal of force exerted by coherence of the sister chromatids reduced fragmentation fourfold. Removal of the forces exerted by the cytoplasmic microtubules had no effect on fragmentation. Our results provide insights into the relative contributions of the kinetochore and cytoplasmic microtubules to the forces involved in formation of a bipolar spindle.

INTRODUCTION

Successful chromosome segregation during cell division in eukaryotes is achieved by the coordinated actions of microtubules and chromosomes. Formation of a bipolar mitotic spindle is essential in this process and requires duplication of the centrosome, the microtubule organizing center of the cell. The two centrosomes organize three classes of microtubules. Kinetochore microtubules attach the chromosomes to the centrosome. Pole-to-pole microtubules emanate from opposite centrosomes and overlap in the spindle midzone, providing structural integrity to the spindle. The astral microtubules make contact with the cell cortex and function to position the spindle. Replicated chromosome pairs become bioriented as sister kinetochores attach to opposite centrosomes via the kinetochore microtubules. Once bioriented, kinetochores are under enough tension to stretch the centromeric chromatin during metaphase (Shelby *et al*., 1996; Waters *et al*., 1996). This tension implies the presence of at least two forces, one toward the centrosomes to stretch the chromatin and a counterforce that prevents spindle collapse. In *Xenopus* egg extracts, microtubule flux provides the force pulling toward the centrosomes (Maddox *et al*., 2003). A proper balance and regulation of the different forces acting in the spindle is necessary for successful delivery of the replicated genome to each daughter cell.

In yeast, the spindle pole body (SPB) is the functional equivalent to the centrosome. The duplicated SPBs nucleate the three classes of microtubules and set up the bipolar spindle. The kinetochores are also under tension and chromatin stretching occurs (Goshima and Yanagida, 2000). However, little if any microtubule flux occurs (Maddox *et al*., 2000). Spindle collapse is prevented by pole-to-pole microtubules exerting an outward force on the SPBs, causing them to remain separated, while kinetochore microtubules exert an inward force, pulling the SPBs together. Cin8p and Kip1p are BimC-type kinesin motors that separate the SPBs and keep them separated (Hoyt *et al*., 1992; Roof *et al*., 1992; Saunders and Hoyt, 1992). The Kar3p motor pulls the SPBs inward (Saunders and Hoyt, 1992). In addition to the motors, the kinetochores and cohesion of the sister chromatids also exert an inward pulling force on the SPBs as evidenced by the longer spindles of kinetochore and cohesin mutants (Guacci *et al*., 1997; Goshima and Yanagida, 2000). Addi-

Article published online ahead of print. Mol. Biol. Cell 10.1091/mbc.E04–08–0703. Article and publication date are available at www.molbiolcell.org/cgi/doi/10.1091/mbc.E04–08–0703.

[D] [V] The online version of this article contains supplemental material at MBC Online (http://www.molbiolcell.org).

§ Corresponding author. E-mail address: tdavis@u.washington.edu.

Abbreviations used: 3-D, three dimensional; CFP, cyan fluorescent protein; EM, electron microscopy; FRET, fluorescence resonance energy transfer; GFP, green fluorescent protein; HU, hydroxyurea; SPB, spindle pole body; YFP, yellow fluorescent protein.

tional forces are exerted on the SPB by the cytoplasmic microtubules, which orient the spindle and pull the nucleus into the bud via two partially redundant pathways, one involving the dynein/dynactin complex and the other involving the kinesin-related Kip3p (Schuyler and Pellman, 2001). The relative contributions of these proteins to forces on the SPB and maintenance of tension on the kinetochore is not known.

The SPB spans the nuclear envelope and is composed of three main layers: the inner plaque in the nucleus, the central plaque in the plane of the nuclear envelope, and the outer plaque in the cytoplasm. Microtubules emanate from the inner and outer plaques of the SPB. Microtubules are nucleated by the γ-tubulin complex (composed of Tub4p [yeast γ-tubulin], Spc98p and Spc97p) (Knop *et al*., 1997; Knop and Schiebel, 1997) The capped minus end of a yeast microtubule is reminiscent of the minus ends of microtubules in *Drosophila*, which are capped with the γ-tubulin ring complex (Moritz *et al*., 2000). Spc72p connects the γ-tubulin complex to the cytoplasmic side of the SPB, whereas Spc110p links the complex to the nuclear side of the SPB (Knop and Schiebel, 1997, 1998; Nguyen *et al*., 1998). The long coiled-coil region of Spc110p extends from the inner plaque to the central plaque (Kilmartin *et al*., 1993). The central plaque is composed of a crystalline array of Spc42p (Bullitt *et al*., 1997). This crystalline array forms a lattice onto which the other SPB core proteins are assembled, including the C-terminal domain of Spc110p, calmodulin and Spc29p. The C terminus of Spc110p binds Spc42p, Spc29p, and calmodulin (Geiser *et al*., 1993; Adams and Kilmartin, 1999; Elliott *et al*., 1999; Vinh *et al*., 2002).

Spc110p has four regions defined by genetic and biochemical analysis. The N-terminal region binds to the γ-tubulin complex (Sundberg and Davis, 1997; Nguyen *et al*., 1998; Vinh *et al*., 2002). The coiled-coil region acts as a spacer between the inner plaque and central plaque (Kilmartin *et al*., 1993). Region II is on the C-terminal side of the coiled-coil and was recognized by a cluster of mutations that disrupt Spc110p function. Finally, region III contains the calmodulin binding site at the very C terminus of the protein. Calmodulin binding to Spc110p is required for proper assembly of Spc110p into the SPB (Sundberg *et al*., 1996; Sundberg and Davis, 1997).

The region II allele *spc110–226* confers temperature sensitivity and loss of viability during mitosis (Sundberg and Davis, 1997). Previous characterization of the mutant phenotype revealed a defect in maintaining SPB integrity after spindle assembly. At early time points in a synchronous shift to the restrictive temperature, short, apparently normal, spindles are seen by electron microscopy. At late time points, the spindles are absent and some of the SPBs look structurally compromised. Immunofluorescence at the late time points reveals three foci containing the Spc98p component of the γ-tubulin complex instead of the usual two SPBs. We hypothesized that the SPB disintegrated due to some force on the spindle. This interesting mutant phenotype provides us with a system to study the molecular structure of the SPB and consequences to the spindle architecture when the balance of forces is disturbed by a weakened SPB. We combine live cell movies, fluorescence localization, fluorescence resonance energy transfer (FRET), high-resolution electron microscopy (EM), tomography, and genetics to fully characterize the mutant phenotype and to study the forces on the SPB that cause fragmentation.

MATERIALS AND METHODS

Media

YPD medium was described previously (Geiser *et al*., 1991). YPD + 3 × Ade is YPD medium supplemented with adenine to a final concentration of 150 μg/ml. SD complete is SD medium (Sherman *et al*., 1986; Davis, 1992) supplemented with 50 μg/ml adenine, 25 μg/ml uracil, 100 μg/ml tryptophan, and 0.1% casamino acids. YCAT medium is SD complete with 0.25% casamino acids. SD-ura is SD complete lacking uracil. SGAL-ura is SD-ura with 2% galactose substituted for glucose.

Strains

Strains used in this study are listed in Table 1. All strains were derived from W303. C-terminal cyan fluorescent protein (CFP), green fluorescent protein (GFP), Venus, and yellow fluorescent protein (YFP) fusions were created by amplifying the CFP-hphMX3, Venus-kanMX6, YFP-HIS3MX6, YFP-kanMX6, or GFP-kanMX6 cassettes from plasmids pBS4, pBS7, pDH5, or pDH6 (all gifts from Yeast Resource Center) or pFA6aGFPS65T-kanMX6 (Wach *et al*., 1997). Each polymerase chain reaction (PCR) cassette was integrated in frame at the 3′ end of the target gene. N-terminal CFP and YFP fusions were created by integrating PCR products amplified from pDH22 and pBS5 (all gifts from Yeast Resource Center, University of Washington, Seattle, WA) at the 5′ end of the target gene, followed by CRE/LOX-mediated excision of the selectable marker to yield an in frame N-terminal CFP or YFP tag (Prein *et al*., 2000). The dynein deletion strain was created by integrating a hygromycin marker amplified from pAG32 (a gift from Yeast Resource Center; Goldstein and McCusker, 1999) in place of the *DYN1* open reading frame. The GFP-tubulin strains were created by integrating *Stu*I-linearized pAFS125 (GFP-TUB1-URA3) at the URA3 locus. To tag Pds1p with HA (*PDS1–3 × HA*), plasmid pOC52 (a gift from V. Guacci, Fox Chase Cancer Center, Philadelphia, PA) was linearized with *Cla*I and *Sac*I and integrated. Integrations were confirmed by microscopy and/or by PCR. The *cdc26*Δ (Araki *et al*., 1992; Zachariae *et al*., 1996), *mcd1–1* (Guacci *et al*., 1997), *ndc10–1* (Goh and Kilmartin, 1993), and *ipl1–321* (Biggins *et al*., 1999) temperature-sensitive alleles have been described previously.

Western Blot Analysis

Membranes were blocked for 1 h in Tris-buffered saline with 0.1% Tween 20 (TBST), 3% nonfat milk, and 3% bovine serum albumin (BSA). Membranes were incubated overnight with mouse monoclonal IgG recognizing hemagglutinin (HA) (clone 12CA5, 1:300; Roche Diagnostics, Indianapolis, IN). After 3 × 10 min washes in TBST, membranes were incubated 1 h with goat anti-mouse IgG, (H+L), horseradish peroxidase conjugated (1:10,000; Pierce Chemical, Rockford, IL) in 1% nonfat milk and 1% BSA. After 3 × 15 min washes in TBST, the membranes were developed using the ECL Plus chemiluminescence system (Amersham Biosciences, Piscataway, NJ); membranes were exposed to Hyperfilm (Amersham Biosciences). Processed films were scanned with an Agfa Arcus II flatbed scanner.

Fluorescence-assisted Cell Sorting Analysis of DNA Content

Yeast cells were prepared for flow cytometry and analyzed for DNA content as described previously (Muller, 1991).

Fluorescence Microscopy of Temperature-shifted Fixed Cells

For fluorescence localization of central plaque proteins, mutant *spc110–226* cells were cultured at 22°C overnight in YPD. *ADE3*, *ade2–1oc* strains accumulate a fluorescent by-product of adenine biosynthesis in the vacuole when adenine is limiting. These strains were cultured in YPD + 3 × Ade to suppress the accumulation of this pigment. Asynchronous cultures at a cell density of ~60 Klett units (1.8×10^7 cells/ml) were shifted to 37°C, and samples of cells were taken at various times. Cells were fixed in 3.7% formaldehyde for 15 min in a 30°C roller drum and washed twice with phosphate-buffered saline (PBS). Cells were either mixed with a solution of 1.5% low melting point agarose in YCAT medium or placed on a pad of PBS 1.5% low melting point agarose and mounted on a microscope slide under a no. 1.5 coverslip. Cells were imaged using a DeltaVision deconvolution microscopy system from Applied Precision (Issaquah, WA), which includes an Olympus IL-70 microscope with a u-plan-apo 100× oil objective (1.35 numerical aperture). A CoolSnap HQ digital camera from Roper Scientific (Tucson, AZ) and optical filter sets from Omega Optical (Battleboro, VT) were used to acquire images. The images were analyzed using DeltaVision softWoRX software. To determine localization of proteins present in the SPB and the aberrant structures, a z-series of nine images at 0.4-μm intervals was acquired. The series was acquired with 0.5-s exposures, first in the YFP channel and then in the CFP channel. Binning on the camera was set to 2 × 2 and the gain was set to 1 or 2.

To characterize spindle morphology during hydroxyurea (HU) arrest, cells were arrested in 0.1 M HU (Sigma-Aldrich, St. Louis, MO) for 4.5 h at room

Table 1. Yeast strains[a] and plasmids used in this study

Strain	Genotype	Source or reference
BESY15-2C	*MAT***a** *CFP::SPC42 SPC110::YFP-HIS3MX6*	Muller *et al.* (manuscript in preparation)
BESY32	*MATα ade3Δ100 CFP::SPC42::YFP-kanMX6*	Muller *et al.* (manuscript in preparation)
BESY41-2D	*MAT***a** *ade3Δ100 SPC29::YFP-kanMX6 CFP::SPC42 TRP1*	Muller *et al.* (manuscript in preparation)
BSY9	*MAT***a***/MATα ADE3/ade3Δ100 CYH2s/cyh2r*	Hazbun *et al.* (2003)
DHY28	*MATα ade3Δ100 SPC29::CFP-kanMX6 SPC110::YFP-HIS3MX6*	Muller *et al.* (manuscript in preparation)
EMY194-2C	*MAT***a** *ade3Δ100 SPC29::YFP-kanMX6 SPC42::CFP-kanMX6 TRP1*	Muller *et al.* (manuscript in preparation)
HSY83	*MAT***a***/MATα ADE3/ade3Δ HIS3/his3-11,1spc110-226/spc110-226*	Sundberg and Davis (1997)
JBY11	*MAT***a***/MATα ADE3/ade3Δ lys2:HIS3/LYS2 MCD1-MYC/MCD1-MYC*	This study
JBY24	*MAT***a***/MATα ADE3/ade3Δ lys2:HIS3/LYS2 PDS1-HA-URA3/PDS1-HA-URA3*	This study
JBY60	*MAT***a***/MATα ADE3/ade3Δ HIS3/his3-11,15 MCD1-MYC/MCD1-MYC PDS1-HA-URA3/PDS1-HA-URA3 spc110-226/spc110-226*	This study
MAMY2	*MAT***a***/MAT***a** *ade3Δ100/ade3Δ100 LYS2/lys2::HIS3 SPC29::YFP-kanMX6/SPC29 SPC97::CFP-hphMX3/SPC97 spc110-226/spc110-226 TRP1/trp1-1*	This study
MAMY3	*MAT***a***/MAT***a** *ade3Δ100/ade3Δ100 LYS2/lys2::HIS3 SPC42::YFP-kanMX6/SPC42 SPC97::CFP-hphMX3/SPC97 spc110-226/spc110-226 TRP1/trp1-1*	This study
MAMY8-1C	*MAT***a** *ade3Δ100 SPC29::CFP-kanMX6 spc110-226::YFP-his5MX6 URA3*	This study
MAMY9-4C	*MAT***a** *ade3Δ100 CFP::SPC42 spc110-226::YFP-HIS3MX6 URA3*	This study
MAMY12-1D	*MAT***a** *ade3Δ100 LEU2 CFP::SPC42::YFP-kanMX6 spc110-226*	This study
MAMY13	*MAT***a** *SPC29::YFP-kanMX6 SPC42::CFP-hphMX3 spc110-226*	This study
MAMY14-5D	*MATα ade3Δ100 lys2Δ::HIS3 SPC29::YFP-kanMX6 CFP::SPC42 spc110-226*	This study
SFY200	*MAT***a***/MAT***a** *ade3Δ100/ade3Δ100 lys2Δ::HIS3/LYS2 spc110-226/spc110-226 TRP1/trp1-1*	This study
SBY918	*MAT***a** *bar1-1 cdc26Δ::kanMX HIS3::CUP1-GFP12lacI12 lys2Δ CENIIIlacO128::TRP1*	
TDY168-7D	*MAT***a** *ade3Δ100 lys2Δ::HIS3 mcd1-1 SPC97::Venus-kanMX6 spc110-226 lacO::TRP1::URA3*	This study
TDY173-27B	*MAT***a** *HIS3::CUP1-GFP12lacI12 lys2Δ spc110-226 CENIIIlacO128::TRP1*	This study
TDY174-29B	*MAT***a** *arp1::TRP1 arp1ts-degron::LEU2 kar9::HIS3MX SPC97::Venus-kanMX spc110-226*	This study
TDY176-2A	*MAT***a** *ade3Δ100 NUF2::Venus-kanMX6 SPC97::CFP-hphMX3 spc110-226 TRP1*	This study
TDY178-1A	*MAT***a** *ade3Δ100 ndc10-1 SPC97::Venus-kanMX6 spc110-226*	This study
TDY179-11D	*MAT***a** *ade3Δ100 ipl1-321 SPC97::Venus-kanMX6 spc110-226 TRP1*	This study
TDY180-16B	*MAT***a** *ade3Δ100 lys2Δ::HIS3 mad1Δ::URA3 SPC97::Venus-kanMX6 spc110-226*	This study
TDY181	*MAT***a** *HIS3::CUP1-GFP12lacI12 lys2Δ mad1Δ::URA3 CENIIIlacO128::TRP1 spc110-226*	This study
TDY182-4B	*MAT***a** *cdc26Δ::kanMX NUF2::Venus-kanMX6 SPC97::CFP-hphMX3 TRP1*	This study
TYY146	*MAT***a***/MATα ade3Δ100/ade3Δ100 LEU2/leu2-3,112 lys2Δ::HIS3/lys2Δ::HIS3 spc110-226/spc110-226 TRP1/trp1-1 GFP-TUB1-URA/GFP-TUB1-URA3*	This study
TYY150	*MAT***a***/MATα GFP-TUB1-URA3/GFP-TUB1-URA3*	This study
TYY154	*MAT***a***/MATα ADE3/ade3Δ100 CYH2s/cyh2r SPC97::GFP-kanMX6/SPC97*	This study
TYY158	*MAT***a***/MATα ADE3/ade3Δ100 dyn1Δ-hphMX3/DYN1 HIS3/his3-11,15 spc110-226/SPC110*	This study
TYY161	*MAT***a***/MAT***a** *ade3Δ100/ade3Δ100 lys2Δ::HIS3/LYS2 NIC96::CFP-hphMX3/NIC96 SPC97::Venus-kanMX6/SPC97 spc110-226/spc110-226 TRP1/trp1-1*	This study
TYY167	*MAT***a***/MATα ade3Δ100/ade3Δ100 LEU2/leu2-3,112 lys2Δ::HIS3/lys2Δ::HIS3 SPC97::GFP-kanMX6/SPC97::GFP-kanMX6 spc110-226/spc110-226 trp1-1/TRP1*	This study
TYY169	*MAT***a** *ade3Δ100 lys2Δ::HIS3 SPC97::Venus-kanMX6 spc110-226*	This study
W303	ade2-loc can1-100 his3-11,15 leu2-3,112 trp1-1 ura3-1	This study
Plasmids		
pGF29	URA3 2 μm vector	G. Zhu, Johns Hopkins University, gift
pKB701	URA3 2 μm vector + GAL-DYN1-GFP	K. Bloom, University of North Carolina, gift
pAFS125	GFP-TUB1-URA3	A. Straight, Stanford University, gift

[a] All strains in this study are of W303 genotype with the exceptions noted.

temperature, fresh 0.1 M HU was added and cells were shifted to 37°C for another 45-min incubation. They were then fixed in formaldehyde and mounted as described above. Z-series of 15 images (0.3-s fluorescein isothiocyanate exposures) at 0.2-μm intervals were acquired. The images were deconvolved before analysis.

Synchronous populations of cells in G1 were obtained as follows. Cultures were grown to 27 Klett units in YPD medium at room temperature (20–22°C). α-factor (4 μM) was added and the cultures were incubated at room temperature for 1.5 generations. Cells were filtered, washed with five volumes YPD, sonicated, and released to 37°C. At each time point, samples were fixed for 15 min in 3.7% formaldehyde at room temperature and washed once in PBS.

Cells were mounted for microscopy in PBS citifluor (Ted Pella, Redding, CA) on a pad of 1% agarose in SD medium under a 1.5 coverslip. To look at kinetochore arrangement, *SPC110* control and *spc110–226* cells carried Nuf2p-Venus and Spc97p-CFP. A z-series of 15 images (0.4-s YFP exposures, 0.3-s CFP exposures, 0.05-s differential interference contrast [DIC] exposures) at 0.4-μm intervals were collected. Biorientation of a single centromere was visualized as separated sister centromeres or stretched chromatin in strains with CENIII tagged with 128 copies of lacO and lacI-GFP integrated at the HIS3 locus. A z-series of 24 images (0.3-s GFP exposures, 0.05-s DIC exposures) at 0.2-μm intervals were collected. SPB fragmentation was visualized with Spc97p-Venus. A z-series of 16 images (0.4-s YFP exposures and 0.05-s

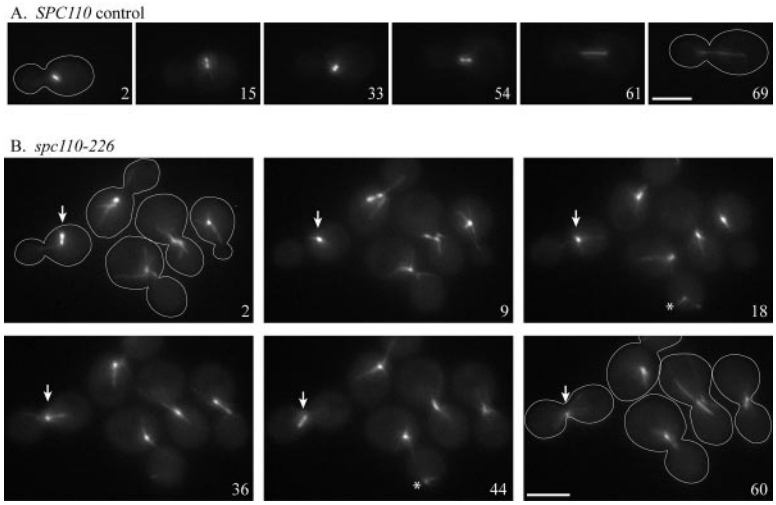

Figure 1. Live cell movies of GFP-Tub1 spindles in wild-type and the *spc110–226* mutant at 37°C (TYY150 and TYY146). Cells were grown at 37°C on a heated microscope stage, and images were collected in 3-D at 1-min intervals. (A) Control *SPC110* cells were observed to progress through anaphase, N = 4. See Supplementary Materials (Video 1) for full movie sequence (79 min). (B) Fracture and collapse of the mutant spindles was observed as well as abnormalities in the cytoplasmic microtubule arrays, N = 22. Arrows point to a spindle that forms, collapses, and reforms. Asterisks point to a fragment of the microtubule array that detaches from the main spindle and moves around in the bud. See Supplementary Materials (Video 2) for full movie sequence (90 min). Bar, 5 μm. Numbers represent time in minutes.

DIC exposures) at 0.4-μm intervals were collected. Cells were scored for the number of spots of Spc97p-Venus per cell. Note that even SPB remnants in which the entire inner plaque is stripped away would still have Spc97p-Venus in the outer plaque. Greater than 100 cells were scored for each time point.

Live Cell Movies at 37°C

Cells were grown at ~22°C on YPD plates. On the day before imaging, cells from a single colony were struck on YPD + 3 × ade plates. Live cells were mounted on a pad of 2% SD complete agarose on a microaqueduct slide in a FCS2 heated microscope slide chamber from Bioptechs (Butler, PA). The 60× Olympus objective was heated using an objective heater from Bioptechs. (The outer collar of the objective was removed to mount the objective heater band.) Cells were incubated 20–40 min at 37°C before the movies were started. Movies were taken of any budded cells in the field that had not entered anaphase. A z-series of seven sections 0.5 μm apart was acquired once each minute. The gain was set to 2, and the images were binned 2 × 2. The softWoRX software was used to measure distance between two spots of Spc97p-GFP fluorescence in three dimensions (3-D).

Fluorescence Resonance Energy Transfer

FRET methodology has been described previously (Hailey *et al*., 2002). Briefly, live cells (N = 125) containing CFP and YFP fusion proteins were mounted on a pad of 1% agarose in SD complete medium on a microscope slide under a no. 1.5 coverslip immediately before imaging. Cells were imaged in single planes under three different filter settings: 1) YFP excitation/YFP emission, 2) CFP excitation/YFP emission (measuring FRET), and 3) CFP excitation/CFP emission. All exposures were 0.4 s. The sum of pixel intensities in a defined region of interest and a manually selected background region of the same size from the same image plane were quantified. A baseline value for the amount of signal expected in the absence of FRET due to spectral spillover between channels was calculated for each cell as the background-corrected CFP signal multiplied by a $\text{Spillover}_{\text{CFP}}$ standardization factor (0.446) plus the background-corrected YFP signal multiplied by a $\text{Spillover}_{\text{YFP}}$ standardization factor (0.232). The spillover factors were determined in cells expressing either CFP- or YFP-tagged proteins alone. The final FRET ratio (FRET_{R}) value for each selected cell was then calculated by dividing the background-corrected FRET value by the total spillover.

Preparation of Cells for Electron Microscopy

Yeast strains were prepared for electron microscopy by using methods described previously (Winey *et al*., 1997; O'Toole *et al*., 1999). Briefly, cells from cultures grown at nonpermissive temperature were collected by vacuum filtration and high pressure frozen by using a Balzers HPM010 high-pressure freezer (BAL-TEC; Technotrade International, Manchester, NH). The frozen cells were freeze substituted in 3% glutaraldehyde and 0.1% uranyl acetate in acetone for 3 d at –90°C then low temperature-embedded in Lowicryl HM20. Serial thick (300- to 400-nm) sections were collected onto Formvar-coated slot grids and poststained in 2% uranyl acetate in 70% methanol followed by Reynold's lead citrate. For tomography, 15-nm colloidal gold particles (Sigma-Aldrich) were affixed to both sides of the grid to serve as alignment markers.

Electron Tomography and Image Analysis

Sections were imaged in a JEOL JEM 1000 high-voltage microscope (JEOL, Peabody, MA) operating at 750 kV. Serial, tilted views were collected about two orthogonal axes every 1.5° over a ± 60° range by using a Gatan 1K × 1K charge-coupled device camera at a pixel size of 1.4 nm. Dual-axis tomographic reconstruction was carried out using the IMOD software package as described in detail previously (Kremer *et al*., 1996; O'Toole *et al*., 2002). Briefly, the serial, tilted views were aligned using the position of the gold particles, and tomograms were computed using R-weighted back projection. The tomograms from each axis were then aligned and combined (Mastronarde, 1997). A total of seven SPBs and eight nuclear microtubule arrays were examined from the *spc110–226* strain.

Tomographic reconstructions were displayed and modeled using the 3dmod viewing program (Kremer *et al*., 1996). Cellular features such as the nuclear envelope, SPBs, and individual microtubules were tracked and modeled. A projection of the model was displayed to determine the structural phenotype of the *spc110–226* strain and to examine the relationships of these structures in 3-D.

Online Supplemental Material

Videos 1 and 2 show live cell movies of wild-type and *spc110–226* mutant (respectively) GFP-Tub1p cells grown at 37°C. Video 3 shows a movie of the projected 3-D model of SPBs and associated structures from the *spc110–226* cell shown in Figure 5A. Videos 4 and 5 show projected 3-D models of intranuclear microtubule arrays from two different *spc110–226* cells shown in Figure 6, A and B. The video sequences associated with Figure 6, C and D, show a movie through the complete tomographic volume of a portion of the cell containing SPBs and a nuclear microtubule aster containing an electron-dense core (Video 6) and the corresponding projected 3-D model from this reconstruction (Video 7).

RESULTS

Initial characterization of the temperature-sensitive *spc110–226* mutant by electron microscopy made the strong prediction that after short spindle formation, at least one of the SPBs disintegrates and the spindle breaks upon incubation at the restrictive temperature (Sundberg and Davis, 1997). To fully characterize the spindle defect conferred by the *spc110–226* mutant, we made movies of *SPC110* control and *spc110–226* cells with GFP-labeled tubulin growing at the restrictive temperature. Control cells were observed to progress through anaphase as expected (Figure 1A and Video 1). The mutant cells were capable of forming a short spindle, but even early in the cell cycle had an abnormally prominent astral microtubule array (Figure 1B and Video 2). Before anaphase a dramatic defect was sometimes observed: fracture of the spindle resulting in a third microtubule array that roamed around in the bud, with dynamically growing and shrinking microtubules. After fracture, the nuclear microtubule array remained active and was occasionally observed to attempt spindle formation for a second time. The movies clearly confirm the prediction based on the EM

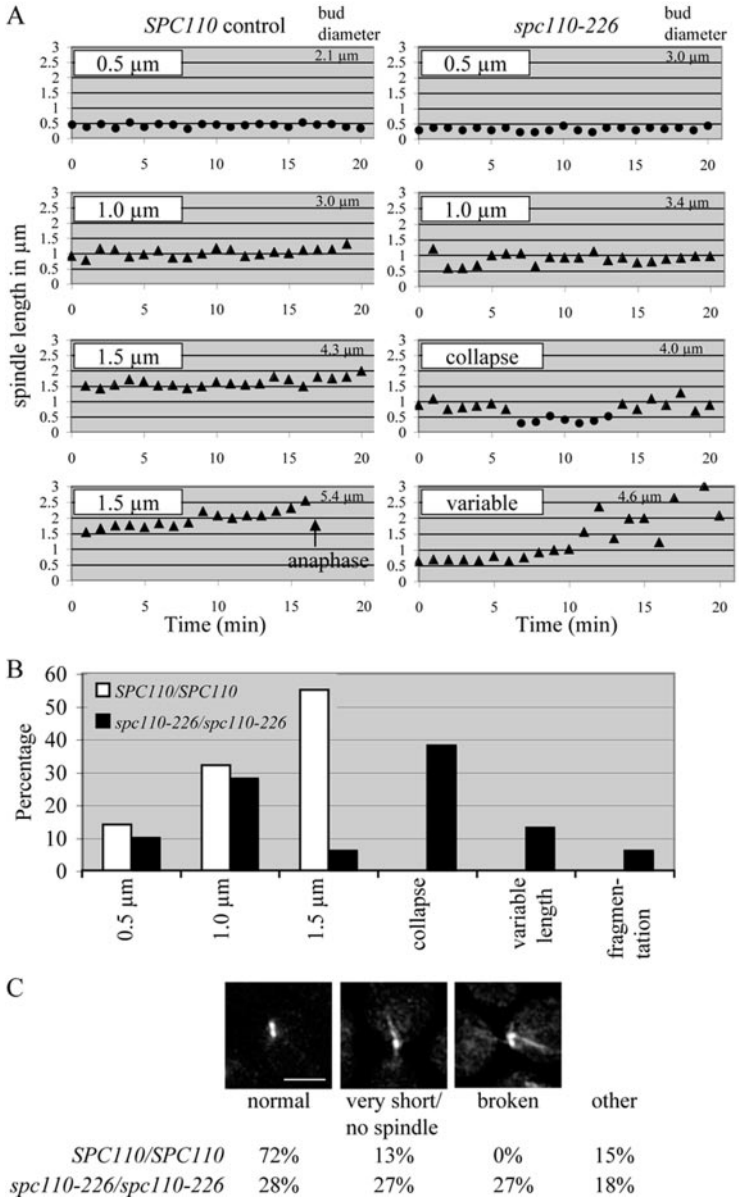

Figure 2. *spc110–226* strains exhibit spindle abnormalities. (A) Control *SPC110* and *spc110–226* diploid cells expressing Spc97p-GFP were preincubated on the heated microscope stage at 37°C for 20–40 min (strains TYY154 and TYY167). Budded cells were identified, and 20-min movies in 3-D were acquired. Spindle lengths were measured in 3-D and plotted over time. Circles represent measurements of SPBs that are not resolved and triangles represent measurements of SPBs that are separated. (B) Percentage of cells exhibiting different spindle phenotypes; N = 32 for *spc110–226* cells and N = 22 for *SPC110* cells. (C) *spc110–226* cells arrested in HU at 37°C exhibit spindle defects. *spc110–226* cells (TYY146) and wild-type controls (TYY150) expressing GFP-Tub1p were arrested in HU at room temperature, and then shifted to 37°C and fresh HU was added (*Materials and Methods*). After incubation for 45 min at 37°C, cells were fixed and imaged by serial sectioning deconvolution fluorescence microscopy. Spindles were classified as being normal, very short/no spindle, broken or other. N = 187 for *spc110–226* cells and N = 61 for *SPC110* cells. Bar, 5 µm.

images: the *spc110–226* mutant allele leads to a dramatic fracture of the spindle at restrictive temperature.

Using a strain with GFP-labeled SPBs, we looked at cells with separated SPBs, including those in early stages of spindle formation. We made short movies at 37°C in 3-D and monitored spindle lengths over time in single budded cells. At 37°C in our background (W303), wild-type cells separate the SPBs to form a 0.5-µm spindle, which lengthens to 1.0 µm and then to a 1.5-µm preanaphase spindle (Figure 2A and Supplementary Figure 1). The 1.5-µm spindle likely corresponds to a metaphase spindle. It is quite stable and lasts for nearly 20 min and then lengthens into an anaphase spindle. Only 6% of the mutant cells achieved a 1.5-µm spindle. Instead, they only attained 1.0-µm spindles, many of which collapsed either for a brief period (1 or 2 min) or for longer (Figure 2B and Supplementary Figure 1). Two mutant spindles were seen to fragment, yielding three spots of Spc97p-GFP fluorescence during the course of the movie. (Cells that contained three spots at the beginning of the movie acquisition were not included in the analysis, and thus the percentage of cells with a fragmented spindle is an underestimate.) These results indicate a defect in maintaining a stable spindle.

We tested whether the mutant cells can maintain a spindle if it is formed under permissive conditions. Cells (GFP-Tub1p) were arrested with short spindles by treatment with HU under permissive conditions and shifted to 37°C for 45 min in the continued presence of HU. Wild-type cells showed 72% normal short spindles that were ~1 µm in length (Figure 2C). Only 28% of *spc110–226* cells had normal spindles, and the remainder were either very short or broken (Figure 2C). Thus, the *spc110–226* mutant can neither form nor maintain a normal metaphase spindle. Measurement of mutant spindles from EM micrographs published previously (Sundberg and Davis, 1997) showed that intact spindles from the early time points at the restrictive temperature averaged 0.74 µm, consistent with the inability to form a normal 1.5-µm metaphase spindle.

Even though the spindle did not seem to progress past the 1.0-µm length, we still wanted to establish whether frag-

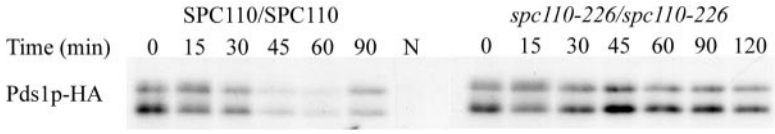

Figure 3. Pds1p remains high in the *spc110–226* arrest. Control *SPC110* (JBY24) and *spc110–226* (JBY60) diploid strains were arrested at 22°C with 0.1 M HU. After 1.5 generations, cells were released to fresh YPD at 37°C where *spc110–226/spc110–226* cells arrested as large budded cells and control cells cycled. Total cellular protein extracts were collected at times indicated after release to 37°C. A Western blot against Pds1p-HA is shown. Pds1p runs as a doublet. The same amount of total protein was loaded in each lane as determined from a Coomassie Blue-stained polyacrylamide gel of the same samples. The negative control (N) is from the untagged strain JBY11.

mentation was triggered by entry into anaphase. One measure of entry into anaphase is a drop in the level of Pds1p in the cell. However, the level of Pds1p remained high in *spc110–226* cells arrested at the restrictive temperature, indicating that fragmentation occurs before entry into anaphase (Figure 3).

The preceding results suggest that the *spc110–226* mutant cells have compromised short spindles and are arrested in a preanaphase cell cycle state. The unstable behavior of the short spindles led us to examine the kinetochore organization by synchronous shifts to 37°C by using a *spc110–226* mutant containing Nuf2p-Venus and Spc97p-CFP (Figure 4A). At 150 min and onward, the cells had either two or three SPB foci, labeled with Spc97p-CFP. Less than 1% of the cells had the normal kinetochore arrangements where all kinetochores are clustered around two SPBs. In ~70% of the cells, all the kinetochores associated with only one SPB, indicating that none of the chromosomes were stably biori-

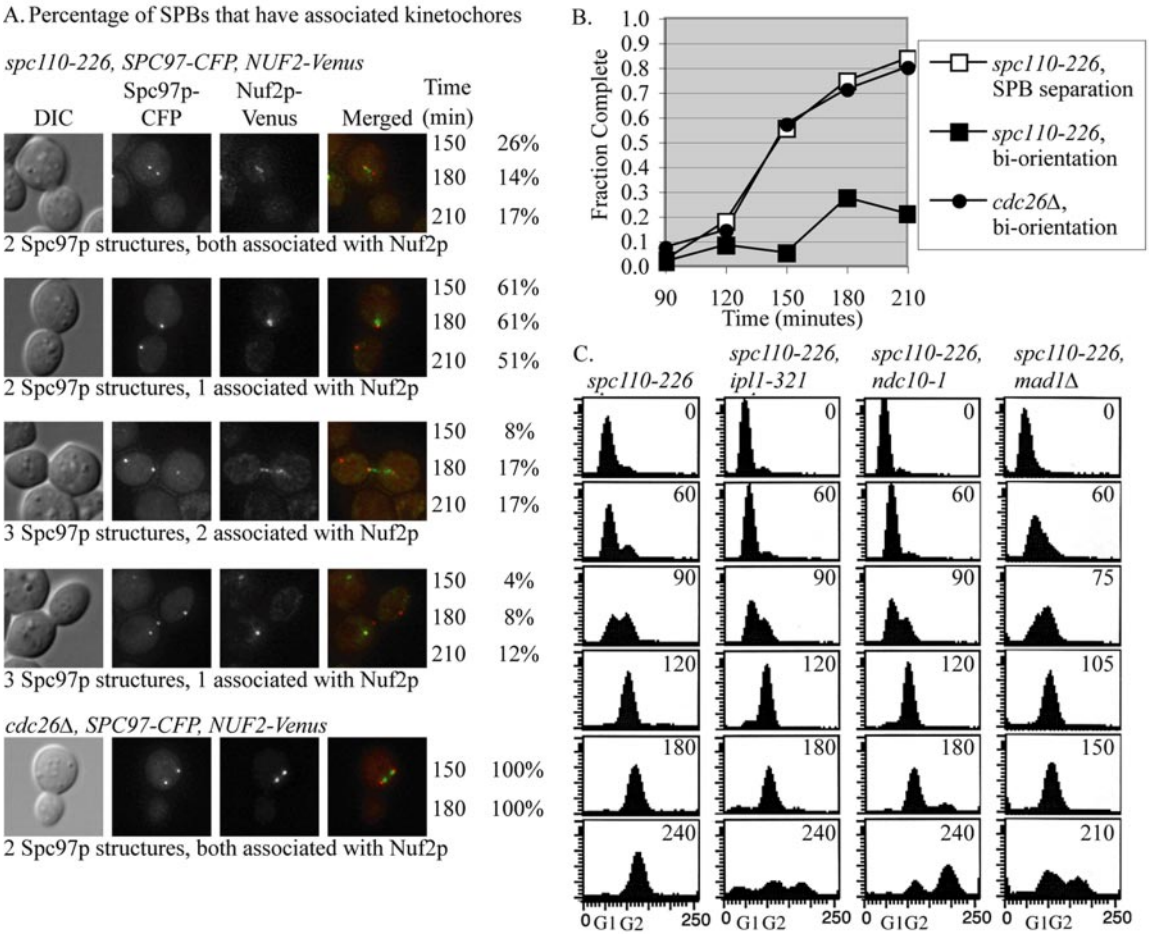

Figure 4. Kinetochores in an *spc110–226* mutant are not arranged properly. (A) *spc110–226* cells with labeled SPBs (Spc97p-CFP) and kinetochores (Nuf2p-Venus) (TDY176–2A) were released from α-factor at 37°C. The percentage of SPBs that had associated kinetochores is reported at 150, 180, and 210 min after shift to the nonpermissive temperature, N = 314 cells. Control *cdc26*Δ cells (TDY182–4B) have 2 SPBs with all kinetochores clustered, N = 145 cells. (B) Kinetochores are not bioriented and stretched in *spc110–226* mutants. *spc110–226* (TDY173–27B) and control *cdc26*Δ (SBY918) cells with GFP lacO integrated at CEN III were released from α-factor at 37°C. At least 100 cells were counted for each time point. The fraction of cells with bioriented chromosome III as visualized by separated centromere spots or stretched centromeres is reported. SPB separation for *spc110–226* was determined using strain TYY169. (C) *spc110–226* (TYY169), *spc110–226, ipl1–321* (TDY179–11D), *spc110–226, ndc10–1* (TDY178–1A) and *spc110–226, mad1*Δ (TDY181) mutants were released from α-factor at 37°C. DNA content and the ability to maintain a checkpoint arrest was analyzed by flow cytometry. Time after release from α-factor is indicated in minutes. The midpoint of S phase (the point at which 50% of the genome is replicated) was the landmark chosen to align the time courses.

ented in these cells (Figure 4A). The majority of SPBs with associated kinetochores were in the mother cell. Control *cdc26*Δ cells arrested with short spindles at the restrictive temperature. One hundred percent of the *cdc26*Δ cells contained two SPBs, each one associated with a cluster of kinetochores (Figure 4A).

The ability of the *spc110–226* to make spindles with bioriented and separated centromeres was used to assess spindle function. In wild-type yeast, chromosomes biorient and then spindle forces stretch the centromeres apart before anaphase (Goshima and Yanagida, 2000; Pearson *et al*., 2001). The separation and biorientation of an individual centromere can be visualized using a strain containing GFP-lacI and an integrated array of lactose repressors (lacO) at the centromere of chromosome III (Straight *et al*., 1996; a gift from Sue Biggins, Fred Hutchinson Cancer Research Center, Seattle, WA). Only 20% of the *spc110–226* mutant cells had spindles with bioriented and separated sister centromere IIIs, whereas 80% of the control *cdc26*Δ cells did (Figure 4B).

Although the kinetochores in the *spc110–226* mutant are not arranged properly, we found evidence that they are sufficiently intact to signal the spindle checkpoint and are occupied by microtubules. First, *spc110–226* single mutants arrested with a G2 content of DNA (Figure 4C). Deletion of *MAD1* or inactivation of the kinetochore (*ndc10–1*) abolishes the arrest (Figure 4C) (Goh and Kilmartin, 1993; Sorger *et al*., 1995). Next, we distinguished whether the spindle checkpoint was activated by lack of tension on the kinetochores or a lack of attachment of microtubules to the kinetochores by monitoring the arrest in an *spc110–226 ipl1–321* double mutant. Failures in tension signal through Ipl1p, but failures in attachment signal independently of Ipl1p (Biggins and Murray, 2001; Pinsky *et al*., 2003). The *spc110–226*, *ipl1–321* double mutant failed to arrest (Figure 4C), suggesting that *spc110–226* confers defects in maintaining tension but not in attaching microtubules to kinetochores.

In summary, although the SPBs can separate in an *spc110–226* mutant and a 1-μm spindle forms, the spindle is not stable and does not achieve a normal 1.5-μm metaphase arrangement. In most cells, the kinetochores are associated with only one SPB, indicating a complete failure in biorientation. Our experiments did not reveal defects in the kinetochores, suggesting that the cause of failed biorientation lies elsewhere.

We used electron tomography of thick sections containing SPBs to visualize these organelles and associated structures in 3-D after arrest of the *spc110–226* mutant cells at the restrictive temperature. Features in the tomograms such as the nuclear envelope, microtubules, and the SPB were modeled. Figure 5 shows selected models of SPBs, nuclear envelope, and associated microtubules from four different cells. In many cells (Figure 5, A–C, and Video 3) few, if any, nuclear microtubules were found attached to the SPB. In these cells, the central plaque of the SPB seemed to bulge outward into the cytoplasm instead of maintaining a position within the plane of the nuclear envelope, as seen in wild-type cells (Video 3; Byers and Goetsch, 1974). Occasionally, SPBs could be found within the plane of the nuclear envelope, and these SPBs had numerous nuclear microtubules (Figure 5D). In contrast, cytoplasmic microtubules could always be detected near the SPB. However, the cytoplasmic microtubules were not directly oriented at the SPB outer plaque, but maintained a position off to one side (Figure 5, A–D, and Video 3).

A close examination of *spc110–226* cells grown at nonpermissive temperature revealed numerous microtubules within the nucleus that were not attached to the SPB (Figure 6, A–D, and Videos 4 and 5). These nuclear microtubules were organized into an aster, with their ends forming a circular arrangement at the center (Videos 4 and 5). In the cell shown in Figure 5C, two SPBs are present that do not contain associated nuclear microtubules. This cell contains a nuclear microtubule array with an electron-dense core at the center of the aster to which microtubule ends seem to converge (Figure 6C, long arrow, and Videos 6 and 7).

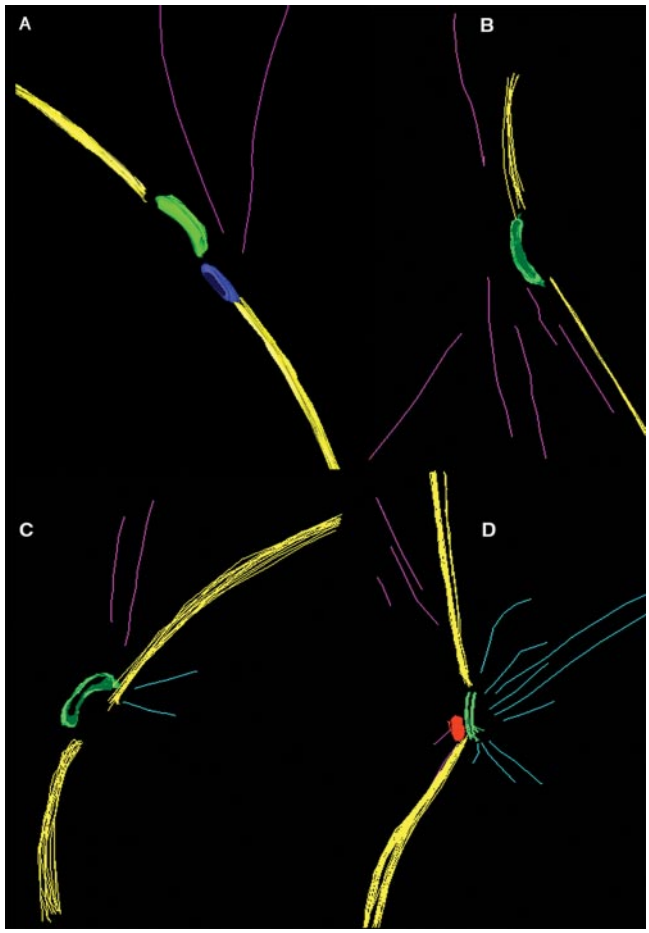

Figure 5. 3-D EM models from *spc110–226* (HSY83) cells show defects in nuclear microtubule attachment and SPB anchoring defects. (A–C) Most cells show few, if any, nuclear microtubules (light blue) attached to the spindle pole body (green). In these cells, the SPB is curved outward into the cytoplasm and is not positioned within the plane of the nuclear envelope (yellow). A mass of electron-dense material could be detected adjacent to the SPB in some cells (A, blue). Video 3 shows a movie of the projected 3-D model in A. (D) An example of a cell containing an SPB with attached nuclear microtubules. (A–D) Cytoplasmic microtubules (pink) were always present, yet look attached toward one side of the SPB.

To study the microtubule ends at the center of the aster more closely, we used a "slicer" tool in the image software. The tool rotates slices of image data, allowing us to follow to a microtubule along its length and examine its end structure in more detail (O'Toole *et al*., 1999). In all cases, the microtubule ends at the center of the aster were capped and often looked pointed (Figure 6, E–I). Filamentous structures could be seen extending from the ends of the microtubules toward the central region of the aster, and in some cases toward an electron-dense core (Figure 6, E–I, arrowhead). A similar morphology has been documented for microtubule minus

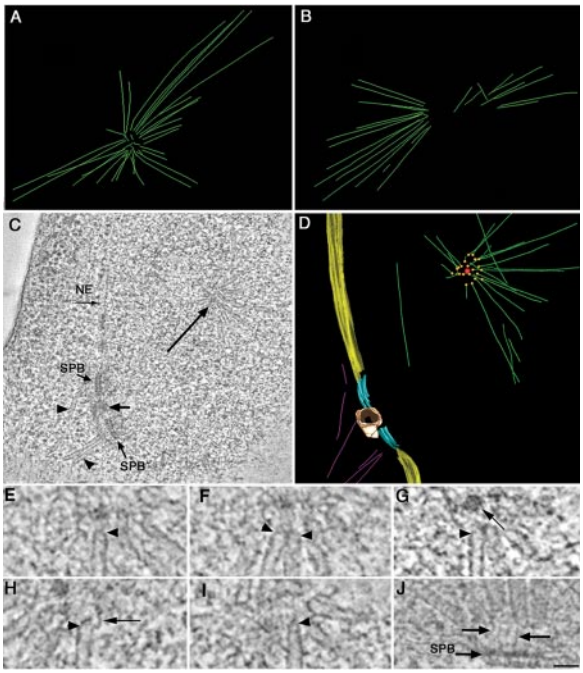

Figure 6. *spc110–226* cells (HSY83) contain an abnormal nuclear microtubule array. (A and B) 3-D EM models show the microtubules form an aster-like array within the nucleus, with their ends converging in a ring at its center. Videos 4 and 5 show the projected 3-D models in A and B. (C) Example of a tomographic slice showing two side-by-side SPBs separated by a mass of electron-dense material (short arrow), nuclear envelope, cytoplasmic microtubules (arrowheads), and a portion of the nuclear microtubule aster containing a spherical core at its center (long arrow). The complete tomographic volume from this cell is shown in Video 6. (D) Projected 3-D model of this cell showing the boundary of the nuclear envelope (yellow) and the SPBs (light blue) separated by an electron-dense mass (tan). Nuclear microtubules (green) are shown forming an aster-like array with their ends (orange spheres) pointed toward a small spherical core (red). Video 7 shows the rotating model. (E–I) Representative images of microtubule ends in nuclear aster arrays from *spc110–226* cells. Microtubule ends pointing toward the center of the aster have a closed, capped morphology (arrowheads). In one example, an electron-dense spherical core could be detected (G; long arrow). Filamentous material could also be seen at the ends of the capped microtubule ends (H, arrow). (J) An example of nuclear microtubules in wild-type cells shows a similar capped morphology (O'Toole *et al*., 1999). Here, however, the nuclear microtubules are tethered to the SPB by fine filaments (arrows). Bar, 50 nm.

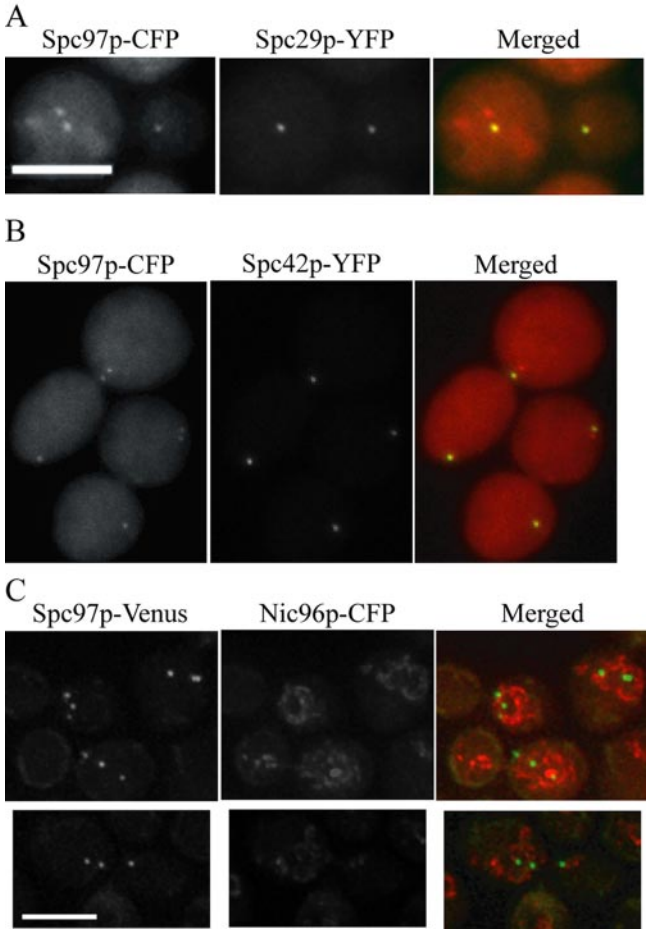

Figure 7. Spc29p-YFP and Spc42p-YFP do not localize to the aberrant structure in the *spc110–226* mutant. (A) Localization of Spc29p-YFP was determined in cells containing Spc97p-CFP after incubation at the nonpermissive temperature for 225 min (MAMY2). Spc29p-YFP localizes to two foci and is absent from the third foci in 100% of the cells, N = 174. (B) Localization of Spc42p-YFP was determined in cells containing Spc97p-CFP after incubation at the nonpermissive temperature for 225 min (MAMY3). Spc42p-YFP localizes to two foci and is absent from the third foci in 100% of the cells, N = 182. (C) Colocalization of the SPBs and/or fragments with the nuclear envelope was determined in cells containing Spc97p-Venus and Nic96p-CFP after incubation at the nonpermissive temperature for 225 min (TYY161). In 94% of cells with three SPBs and/or fragments, all three entities seemed to either colocalize with the nuclear envelope or lie within the nucleus, N = 64. Bar, 5 μm.

ends at the SPB in wild-type cells and the filaments probably correspond to the central coiled-coil domain of Spc110p (Figure 6J; O'Toole *et al*., 1999). However, in wild-type cells, the filamentous structures tether the nuclear microtubule minus ends to the SPB central plaque (Figure 6J, arrows).

The tomograms revealed an aberrant nucleating center located in the nucleoplasm. Previously, we showed by fluorescence microscopy that at the nonpermissive temperature, *spc110–226* mutant cells organize Spc110–226p, calmodulin, and the γ-tubulin complex into three structures (Sundberg and Davis, 1997). Thus, the aberrant structure seen in the tomograms likely corresponds to a complex containing Spc110–226p, calmodulin, and the γ-tubulin complex. We performed fluorescence microscopy to determine what other central plaque components were present in the aberrant structure. Spc29p-YFP and Spc42p-YFP are present in only two of the three structures (Figure 7, A and B), indicating that the SPB breaks at the connection between Spc110–226p and the central plaque components Spc29p and Spc42p.

Tomography also revealed that the SPB remnant associated with the nuclear envelope bulges out on the cytoplasmic face of the nuclear envelope. We performed colocalization of Spc97p-Venus and Nic96p-CFP (a nuclear pore component that localizes to the nuclear envelope) at the restrictive temperature. Spc97p-Venus remained associated with the nuclear envelope or within the nucleus in 94% of the cells (Figure 7C). Therefore although the remnant bulges out, it is not released into the cytoplasm. We conclude that Spc110–226p is found in three structures under nonpermissive conditions: two SPB remnants in the nuclear envelope, including Spc42p and Spc29p, and a nucleating structure with calmodulin and the inner plaque in the nucleoplasm.

Table 2. FRET signals

Strain	FRET donor	FRET acceptor	$FRET_R$	SD
1. DHY28	Spc29p-CFP	Spc110p-YFP	1.32	±0.13
2. MAMY8-1C[a]	Spc29p-CFP	Spc110-226p-YFP	1.42	±0.18
3. BESY15-2C	CFP-Spc42p	Spc110p-YFP	1.84	±0.26
4. MAMY9-4C[a]	CFP-Spc42p	Spc110-226p-YFP	1.40	±0.17
5. BESY32	CFP-Spc42p(−YFP)	(CFP−)Spc42p-YFP	1.16	±0.12
6. MAMY12-1D[a]	CFP-Spc42p(−YFP)	(CFP−)Spc42p-YFP	1.23	±0.11
7. EMY194-2C	Spc42p-CFP	Spc29p-YFP	1.25	±0.15
8. MAMY13[a]	Spc42p-CFP	Spc29p-YFP	1.29	±0.11
9. BESY41-2D	CFP-Spc42p	Spc29p-YFP	1.75	±0.17
10. MAMY14-5D[a]	CFP-Spc42p	Spc29p-YFP	1.65	±0.20

[a] These strains carry the *spc110-226* allele.

Our fluorescence localization studies suggest that the interactions between Spc110p and the central plaque proteins Spc29p and Spc42p are weakened in the *spc110–226* mutant. We analyzed the structure of the mutant SPB under permissive conditions in greater detail by using FRET. The components of the central plaque were tagged with CFP and YFP and energy transfer measured as described in *Materials and Methods*. The energy transfer between CFP-Spc42p and Spc110p-YFP was significantly less in the mutant than in the wild-type strain (Table 2). Thus, the relative arrangement of Spc42p and Spc110–226p is altered even under permissive conditions. No other differences were detected between mutant and wild-type SPBs (Table 2).

At the time that the metaphase spindle is formed, several forces are acting on the spindle. Dynein is pulling on the cytoplasmic microtubules to move the nucleus to the bud. The kinetochores exert tension on the kinetochore microtubules, pulling the SPBs inward, and the cohesin is holding the sister chromatids together. We tested whether altering any of these forces could prevent disintegration and rescue the mutant. Deletion of *DYN1* did not substantially rescue *spc110–226* at the nonpermissive temperature (Figure 8A). Overexpression of dynein had only a very minor synthetic lethal effect on *spc110–226* (Figure 8B). Thus, the force exerted on the SPB through the action of dynein is not the primary cause of SPB fragmentation and spindle fracture.

The effect of removing the outward force was further analyzed using an *arp1*Δ *arp1*^{td} *kar9*Δ temperature-sensitive double mutant to inactivate both the dynein and the Kip3p dependent nuclear positioning pathways (reviewed in Schuyler and Pellman, 2001). In a synchronized shift to the restrictive temperature, *spc110–226 arp1*Δ *arp1*^{td} *kar9*Δ triple mutants showed similar levels of SPB fragmentation as *spc110–226* single mutants; ~40% had three foci of Spc97p-Venus (Figure 8C). Thus, the force exerted on the cytoplasmic face of the SPB during nuclear positioning in the bud neck is not the force responsible for fragmentation of the weakened *spc110–226* SPB.

Tension was released from the kinetochore microtubules by inactivation of cohesin by using the *mcd1–1* temperature-sensitive mutant. In a synchronized shift to the restrictive temperature, only 12% of double mutant *spc110–226 mcd1–1* cells contained three foci of Spc97p-Venus (Figure 8D). In the *spc110–226* single mutant strain, 41% of the cells contained three foci of Spc97p-Venus (Figure 8D). These results indicate that tension exerted on the SPB by the cohered DNA, via the kinetochore microtubules, is largely responsible for the observed SPB fragmentation.

DISCUSSION

One of the initial observations of the *spc110–226* mutant was that it yielded three foci containing Spc110–226p, calmodulin, and the γ-tubulin complex. In this study, we have defined the nature and composition of the three foci. At the restrictive temperature, most of the Spc110–226p, calmodulin, and the inner plaque of the SPB are sheared off, leaving behind Spc29p and Spc42p. This is probably due to the weaker interaction of Spc110–226p with Spc42p, found by FRET analysis. The SPB remnant, bereft of its inner plaque, but containing central plaque components Spc29p and Spc42p, remains associated with the nuclear envelope. Loss of Spc110–226p from the Spc42p crystalline core (Bullitt *et al*., 1997) may change the 3-D structure of the remaining proteins and allow bulging toward the cytoplasm. The misshapen SPB remains anchored in the nuclear envelope. Just like the whole SPB, the detached inner plaque material retains the capacity to nucleate or anchor microtubules that are capped at the minus ends. The tethering of nuclear microtubules into an aster probably results from the ability of the C terminus of Spc110p to self-associate (Kilmartin and Goh, 1996), a property that is not perturbed in the *spc110–226* mutant.

Live cell imaging using GFP-Tub1p or Spc97p-GFP revealed that normal 1.5-μm metaphase spindles do not form in the *spc110–226* mutant cells. The mutant spindles achieve the 1.0-μm stage (prometaphase) but do not elongate and frequently collapse. The unstable spindles are reminiscent of the type of spindles observed in live cell images of kinetochore mutants (Pearson and Bloom, personal communication). Our results suggest that a strong attachment at the SPB is required to form a stable spindle.

In the mutant spindles, the kinetochores are in disarray long before the appearance of a third SPB foci. Many SPBs have no kinetochores associated with them. However, the kinetochores are sufficiently intact to signal the spindle checkpoint and seem to be occupied by microtubules because the Mad1p checkpoint is not triggered in an *spc110–226 ipl1–321* mutant.

We propose that biorientation of the sister chromatids is a key event in fragmentation of the SPB. Biorientation occurs at a low level in the mutant but is not maintained. After SPB separation, the tension that arises from biorientation of a chromosome pulls a small fragment containing Spc110–226p from the SPB. The released Spc110–226p remains attached to the microtubule via the γ-tubulin complex and thereby stabilizes the microtubule minus

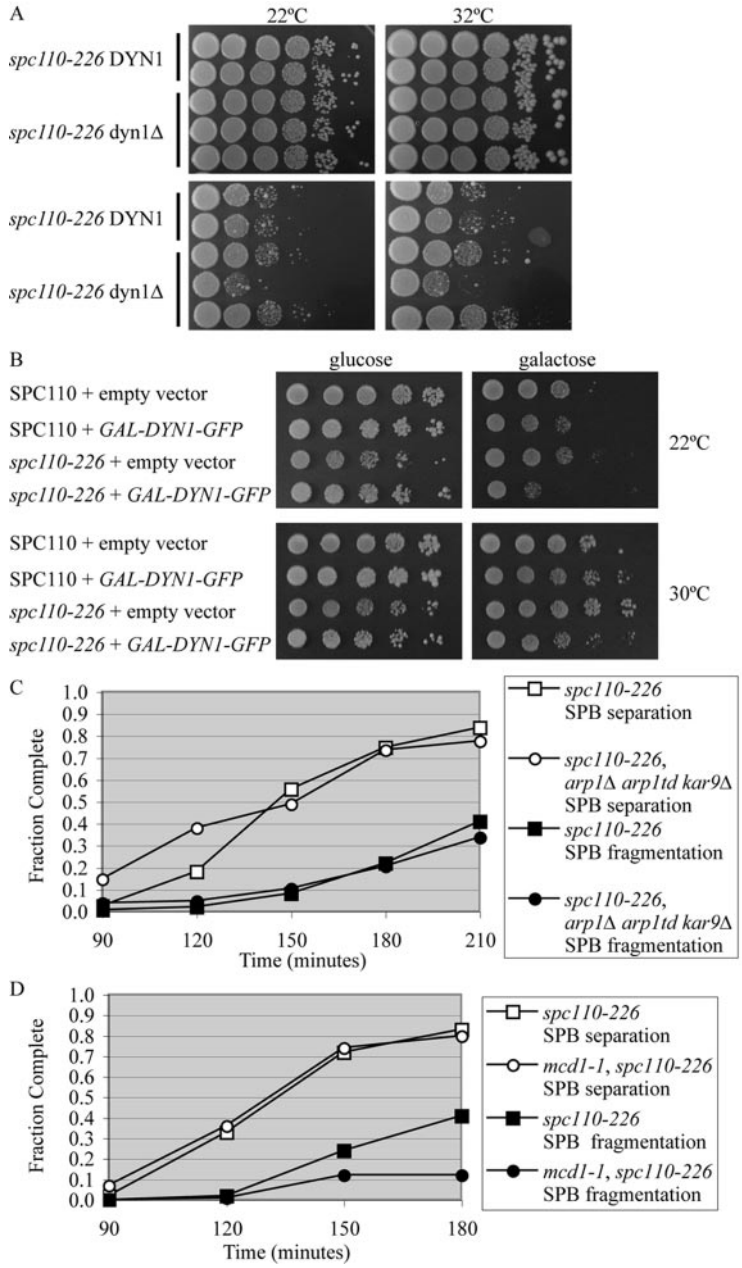

Figure 8. Contribution of cytoplasmic and nuclear forces to SPB fragmentation. (A) Serial dilutions of *spc110–226* haploid cells with either *DYN1* or *dyn1*Δ (derived from TYY158). Independent isolates of the strains were serially diluted (10-fold), spotted on YPD plates, and incubated at 22, 32, 34, and 37°C. (B) Serial dilutions of control *SPC110* (BSY9) and *spc110–226* (SFY200) diploid cells transformed with empty vector (pGF29) or *GAL*-DYN1-GFP (pKB701). Cells were serially diluted (5-fold) and spotted on SD-URA and SGAL-URA. (C) SPB separation (appearance of two or three foci containing Spc97p-Venus) and SPB fragmentation (appearance of three foci containing Spc97p-Venus) were measured in *spc110–226* (TYY169) and *spc110–226*, *arp1*Δ *arp1*^{td} *kar9*Δ (TDY174–29B) cells released from α-factor to 37°C. Time is in minutes after release to 37°C. Greater than 100 cells were counted for each time point. Both Arp1p and Kar9p were inactivated because 92% of the SPBs, and SPB fragments were in the mother cell in the *spc110–226*, *arp1*Δ *arp1*^{td} *kar9*Δ strain, compared with 55% in the mother cell of the *spc110–226* strain. (D) SPB separation and fragmentation were measured in *spc110–226* (TYY169) and *mcd1–1*, *spc110–226* (TDY168–7D) cells with labeled SPBs (Spc97p-Venus) released from α-factor to 37°C. Time is in minutes after release to 37°C. Greater than 100 cells were counted for each time point.

end, whereas the microtubule plus end remains attached to the kinetochore. Once a critical mass of Spc110–226p has been pulled from the SPBs, it coalesces into a visible structure in the nucleus (the aster seen in the tomograms and the foci seen by fluorescence microscopy). The *spc110–226* aster may be a version of the spheroidal polymer that self-assembles in the nucleus when Spc110p is overexpressed (Kilmartin and Goh, 1996).

Why does the disintegration of the spindle only result in three SPB foci and not four or more? In the past, we had presumed that at nonpermissive temperature only the newly assembled SPB is defective and fragments. However, our results show that even when both SPBs were preassembled at the permissive temperature in HU, a normal short spindle is not maintained when shifted to the restrictive temperature. This demonstrates that the SPB does not benefit from being assembled at the permissive temperature. Moreover, the tomograms revealed cells in which both old and new SPBs were structurally compromised. Given the recent result that half of the Spc110p in the old SPB is incorporated after SPB duplication (Yoder *et al*., 2003), we conclude that the preexisting Spc110–226p assembled at permissive temperature is not capable of protecting the old SPB from fragmentation. We envision that the Spc110–226p is removed from the SPB in small bundles attached to the end of a kinetochore microtubule. Only after these fragments aggregate through the self-association of Spc110–226p does the third structure occur.

Our analysis of the role of different forces in SPB fragmentation has revealed the relative contributions of these forces in spindles. The forces that separate the duplicated SPBs are

not sufficient to cause fragmentation. The forces generated by the cytoplasmic microtubules either do not translate across the SPB or are not strong enough to fragment the SPB during spindle orientation and positioning. The cytoplasmic microtubules are likely responsible for the distortion of the SPB remnant into the cytoplasm once most Spc110–226p has been removed. However, the forces anchoring the SPB into the nuclear membrane resist the tearing of the SPB remnant out of the envelope. Sister chromatid cohesion contributes to fragmentation, and relief of this force by inactivation of cohesion decreases fragmentation. Future analyses will take advantage of SPB fragmentation to identify other factors regulating spindle forces.

ACKNOWLEDGMENTS

We thank Sue Biggins for many helpful discussions; the *ipl1–321*, *mcd1–1*, *ndc10–1*, and *cdc26*Δ alleles in a W303 background; strain SBY918; and a strain with CENIII tagged. We thank David Pellman for the *arp1*Δ *arp1tsdegron kar9*Δ mutations in a W303 background. We thank Kerry Bloom, Vincent Guacci, Aaron Straight, the Yeast Resource Center, and Gefeng Zhu for sharing plasmids and reagents. This work was funded by National Institutes of Health R01 GM40506 (to T. D.), National Institutes of Health P41 RR 11823 (to T. D.), and National Institutes of Health R01 GM51312 (to M. W.). The Boulder Laboratory for the 3-D EM of cells is supported by the National Institutes of Health grant RR-00592 to J. R. McIntosh.

REFERENCES

Adams, I. R., and Kilmartin, J. V. (1999). Localization of core spindle pole body (SPB) components during SPB duplication in *Saccharomyces cerevisiae*. J. Cell Biol. *145*, 809–823.

Araki, H., Awane, K., Ogawa, N., and Oshima, Y. (1992). The CDC26 gene of *Saccharomyces cerevisiae* is required for cell growth only at high temperature. Mol. Gen. Genet. *231*, 329–331.

Biggins, S., and Murray, A. W. (2001). The budding yeast protein kinase Ipl1/Aurora allows the absence of tension to activate the spindle checkpoint. Genes Dev. *15*, 3118–3129.

Biggins, S., Severin, F. F., Bhalla, N., Sassoon, I., Hyman, A. A., and Murray, A. W. (1999). The conserved protein kinase Ipl1 regulates microtubule binding to kinetochores in budding yeast. Genes Dev. *13*, 532–544.

Bullitt, E., Rout, M. P., Kilmartin, J. V., and Akey, C. W. (1997). The yeast spindle pole body is assembled around a central crystal of Spc42p. Cell *89*, 1077–1086.

Byers, B., and Goetsch, L. (1974). Duplication of spindle plaques and integration of the yeast cell cycle. Cold Spring Harb. Symp. Quant. Biol. *38*, 123–131.

Davis, T. N. (1992). Mutational analysis of calmodulin in *Saccharomyces cerevisiae*. Cell Calcium *13*, 435–444.

Elliott, S., Knop, M., Schlenstedt, G., and Schiebel, E. (1999). Spc29p is a component of the Spc110p subcomplex and is essential for spindle pole body duplication. Proc. Natl. Acad. Sci. USA *96*, 6205–6210.

Geiser, J. R., Sundberg, H. A., Chang, B. H., Muller, E. G., and Davis, T. N. (1993). The essential mitotic target of calmodulin is the 110-kilodalton component of the spindle pole body in *Saccharomyces cerevisiae*. Mol. Cell. Biol. *13*, 7913–7924.

Geiser, J. R., van-Tuinen, D., Brockerhoff, S. E., Neff, M. M., and Davis, T. N. (1991). Can calmodulin function without binding calcium? Cell *65*, 949–959.

Goh, P. Y., and Kilmartin, J. V. (1993). NDC *10*, a gene involved in chromosome segregation in *Saccharomyces cerevisiae*. J. Cell Biol. *121*, 503–512.

Goldstein, A. L., and McCusker, J. H. (1999). Three new dominant drug resistance cassettes for gene disruption in *Saccharomyces cerevisiae*. Yeast *15*, 1541–1553.

Goshima, G., and Yanagida, M. (2000). Establishing biorientation occurs with precocious separation of the sister kinetochores, but not the arms, in the early spindle of budding yeast. Cell *100*, 619–633.

Guacci, V., Koshland, D., and Strunnikov, A. (1997). A direct link between sister chromatid cohesion and chromosome condensation revealed through the analysis of MCD1 in *S. cerevisiae*. Cell *91*, 47–57.

Hailey, D. W., Davis, T. N., and Muller, E. G. (2002). Fluorescence resonance energy transfer using color variants of green fluorescent protein. Methods Enzymol. *351*, 34–49.

Hazbun, T. R., *et al*. (2003). Assigning function to yeast proteins by integration of technologies. Mol. Cell *12*, 1353–1365.

Hoyt, M. A., He, L., Loo, K. K., and Saunders, W. S. (1992). Two *Saccharomyces cerevisiae* kinesin-related gene products required for mitotic spindle assembly. J. Cell Biol. *118*, 109–120.

Kilmartin, J. V., Dyos, S. L., Kershaw, D., and Finch, J. T. (1993). A spacer protein in the *Saccharomyces cerevisiae* spindle poly body whose transcript is cell cycle-regulated. J. Cell Biol. *123*, 1175–1184.

Kilmartin, J. V., and Goh, P. Y. (1996). Spc110p: assembly properties and role in the connection of nuclear microtubules to the yeast spindle pole body. EMBO J. *15*, 4592–4602.

Knop, M., Pereira, G., Geissler, S., Grein, K., and Schiebel, E. (1997). The spindle pole body component Spc97p interacts with the gamma-tubulin of *Saccharomyces cerevisiae* and functions in microtubule organization and spindle pole body duplication. EMBO J. *16*, 1550–1564.

Knop, M., and Schiebel, E. (1997). Spc98p and Spc97p of the yeast gamma-tubulin complex mediate binding to the spindle pole body via their interaction with Spc110p. EMBO J. *16*, 6985–6995.

Knop, M., and Schiebel, E. (1998). Receptors determine the cellular localization of a gamma-tubulin complex and thereby the site of microtubule formation. EMBO J. *17*, 3952–3967.

Kremer, J. R., Mastronarde, D. N., and McIntosh, J. R. (1996). Computer visualization of three-dimensional image data using IMOD. J. Struct. Biol. *116*, 71–76.

Maddox, P., Straight, A., Coughlin, P., Mitchison, T. J., and Salmon, E. D. (2003). Direct observation of microtubule dynamics at kinetochores in *Xenopus* extract spindles: implications for spindle mechanics. J. Cell Biol. *162*, 377–382.

Maddox, P. S., Bloom, K. S., and Salmon, E. D. (2000). The polarity and dynamics of microtubule assembly in the budding yeast *Saccharomyces cerevisiae*. Nat. Cell Biol. *2*, 36–41.

Mastronarde, D. N. (1997). Dual-axis tomography: an approach with alignment methods that preserve resolution. J. Struct. Biol. *120*, 343–352.

Moritz, M., Braunfeld, M. B., Guenebaut, V., Heuser, J., and Agard, D. A. (2000). Structure of the gamma-tubulin ring complex: a template for microtubule nucleation. Nat. Cell Biol. *2*, 365–370.

Muller, E.G.D. (1991). Thioredoxin deficiency in yeast prolongs S phase and shortens the G1 interval of the cell cycle. J. Biol. Chem. *266*, 9194–9202.

Nguyen, T., Vinh, D.B.N., Crawford, D. K., and Davis, T. N. (1998). A genetic analysis of interactions with Spc110p reveals distinct functions of Spc97p and Spc98p, components of the yeast gamma-tubulin complex. Mol. Biol. Cell *9*, 2201–2216.

O'Toole, E. T., Winey, M., and McIntosh, J. R. (1999). High-voltage electron tomography of spindle pole bodies and early mitotic spindles in the yeast *Saccharomyces cerevisiae*. Mol. Biol. Cell *10*, 2017–2031.

O'Toole, E. T., Winey, M., McIntosh, J. R., and Mastronarde, D. N. (2002). Electron tomography of yeast cells. Methods Enzymol. *351*, 81–95.

Pearson, C. G., Maddox, P. S., Salmon, E. D., and Bloom, K. (2001). Budding yeast chromosome structure and dynamics during mitosis. J. Cell Biol. *152*, 1255–1266.

Pinsky, B. A., Tatsutani, S. Y., Collins, K. A., and Biggins, S. (2003). An Mtw1 complex promotes kinetochore biorientation that is monitored by the Ipl1/Aurora protein kinase. Dev. Cell *5*, 735–745.

Prein, B., Natter, K., and Kohlwein, S. D. (2000). A novel strategy for constructing N-terminal chromosomal fusions to green fluorescent protein in the yeast *Saccharomyces cerevisiae*. FEBS Lett. *485*, 29–34.

Roof, D. M., Meluh, P. B., and Rose, M. D. (1992). Kinesin-related proteins required for assembly of the mitotic spindle. J. Cell Biol. *118*, 95–108.

Saunders, W. S., and Hoyt, M. A. (1992). Kinesin-related proteins required for structural integrity of the mitotic spindle. Cell *70*, 451–458.

Schuyler, S. C., and Pellman, D. (2001). Search, capture and signal: games microtubules and centrosomes play. J. Cell Sci. *114*, 247–255.

Shelby, R. D., Hahn, K. M., and Sullivan, K. F. (1996). Dynamic elastic behavior of alpha-satellite DNA domains visualized in situ in living human cells. J. Cell Biol. *135*, 545–557.

Sherman, F., Fink, G. R., and Hicks, J. B. (1986). Methods in Yeast Genetics. Cold Spring Harbor Laboratory: Cold Spring Harbor, New York.

Sorger, P. K., Doheny, K. F., Hieter, P., Kopski, K. M., Huffaker, T. C., and Hyman, A. A. (1995). Two genes required for the binding of an essential *Saccharomyces cerevisiae* kinetochore complex to DNA. Proc. Natl. Acad. Sci. USA *92*, 12026–12030.

Straight, A. F., Belmont, A. S., Robinett, C. C., and Murray, A. W. (1996). GFP tagging of budding yeast chromosomes reveals that protein-protein interactions can mediate sister chromatid cohesion. Curr. Biol. *6*, 1599–1608.

Sundberg, H. A., and Davis, T. N. (1997). A mutational analysis identifies three functional regions of the spindle pole component Spc110p in *Saccharomyces cerevisiae*. Mol. Biol. Cell *8*, 2575–2590.

Sundberg, H. A., Goetsch, L., Byers, B., and Davis, T. N. (1996). Role of calmodulin and Spc110p interaction in the proper assembly of spindle pole body components. J. Cell Biol. *133*, 111–124.

Vinh, D. B., Kern, J. W., Hancock, W. O., Howard, J., and Davis, T. N. (2002). Reconstitution and characterization of budding yeast gamma-tubulin complex. Mol. Biol. Cell *13*, 1144–1157.

Wach, A., Brachat, A., Alberti-Segui, C., Rebischung, C., and Philippsen, P. (1997). Heterologous HIS3 marker and GFP reporter modules for PCR-targeting in *Saccharomyces cerevisiae*. Yeast *13*, 1065–1075.

Waters, J. C., Skibbens, R. V., and Salmon, E. D. (1996). Oscillating mitotic newt lung cell kinetochores are, on average, under tension and rarely push. J. Cell Sci. *109*, 2823–2831.

Winey, M., Yarar, D., Giddings, T. H., Jr., and Mastronarde, D. N. (1997). Nuclear pore complex number and distribution throughout the *Saccharomyces cerevisiae* cell cycle by three-dimensional reconstruction from electron micrographs of nuclear envelopes. Mol. Biol. Cell *8*, 2119–2132.

Yoder, T. J., Pearson, C. G., Bloom, K., and Davis, T. N. (2003). The *Saccharomyces cerevisiae* spindle pole body is a dynamic structure. Mol. Biol. Cell *14*, 3494–3505.

Zachariae, W., Shin, T. H., Galova, M., Obermaier, B., and Nasmyth, K. (1996). Identification of subunits of the anaphase-promoting complex of *Saccharomyces cerevisiae*. Science *274*, 1201–1204.